PLANT IMMUNITY

A canonical protein complex controls immune homeostasis and multipathogen resistance

Yue Wu[1,2]†, Weiying Xu[1,2]†, Guoyan Zhao[1,3]†, Ziyao Lei[1,2]†, Kui Li[4]†, Jiyun Liu[1]†, Shijia Huang[5], Junli Wang[6], Xiangbin Zhong[1]‡, Xin Yin[1]§, Yuandong Wang[1,3], Haochen Zhang[1,3], Yang He[1], Zian Ye[4], Yonggang Meng[7,8], Xiaoyu Chang[7,8], Hui Lin[1], Xin Wang[1], Yuanyuan Gao[1], Jijie Chai[5], Jane E. Parker[6], Yiwen Deng[1,9]*, Yu Zhang[1]*, Mingjun Gao[4]*, Zuhua He[1]*

The calcium (Ca^{2+}) sensor ROD1 (RESISTANCE OF RICE TO DISEASES1) is a master regulator of immunity in rice. By screening suppressors of *rod1* mutants, we show that ROD1 governs immune homeostasis by surveilling the activation of a canonical immune pathway. Mutations in *OsTIR* (*TIR-only protein*), *OsEDS1* (*enhanced disease susceptibility 1*), *OsPAD4* (*phytoalexin deficient 4*), and *OsADR1* (*activated disease resistance 1*) all abolish enhanced disease resistance of *rod1* plants. OsTIR catalyzes the production of second messengers 2′-(5″-phosphoribosyl)-5′-adenosine monophosphate (pRib-AMP) and diphosphate (pRib-ADP), which trigger formation of an OsEDS1-OsPAD4-OsADR1 (EPA) immune complex. ROD1 interacts with OsTIR and inhibits its enzymatic activity, whereas mutation of *ROD1* leads to constitutive activation of the EPA complex. Thus, we unveil an immune network that fine-tunes immune homeostasis and multipathogen resistance in rice.

Plants have evolved elaborate immune networks, which prioritize growth and reproduction in the absence of pathogens while enabling rapid and robust defense responses upon pathogen infection (*1*–*4*). The plant immune machinery is a two-tiered system (*5*, *6*). Cell surface–localized pattern recognition receptors (PRRs) recognize conserved pathogen-associated molecular patterns (PAMPs) and induce pattern-triggered immunity (PTI), whereas intracellular nucleotide-binding leucine-rich repeat receptors (NLRs) detect pathogen virulence effectors and activate effector-triggered immunity (ETI) (*6*–*8*). PTI and ETI pathways interact with each other, resulting in a coordinated and robust defense against diverse pathogens (*9*–*12*). NLRs are broadly grouped into three subclasses: Toll/interleukin-1 receptor (TIR) NLRs (TNLs), coiled-coil (CC) NLRs (CNLs), and RPW8-like CC domain NLRs (RNLs) (*13*–*15*). TNLs are part of a broader family of TIR-containing proteins, which differs between dicots and monocots (*16*). Both lineages possess TIR-NB-ARC-tetratricopeptide repeat (TNP) and TIR-only proteins, but monocots lack TNLs (*16*, *17*). Pathogen-activated TNLs and induced TIR-only proteins exhibit nicotinamide adenine dinucleotide glycohydrolase (NADase) activity (*18*–*22*). These TIR enzymes produce 2′-(5″-phosphoribosyl)-5′-adenosine monophosphate/5′-adenosine diphosphate (pRib-AMP/ADP) and di-ADP ribose/ADP-ribosylated adenosine triphosphate (di-ADPR/ADPr-ATP) signals that bind to and induce a conformational change in their respective EDS1-PAD4 and EDS1–senescence-associated gene 101 (SAG101) heterodimer receptors (*21*, *22*). The small molecule–bound *Arabidopsis* EDS1-PAD4 and EDS1-SAG101 dimers recruit the downstream RNLs ADR1 and NRG1 to promote immunity and host cell death, respectively (*21*–*23*). Whether and how TIR-containing proteins function in the control of monocot plant immunity remains elusive.

The rice Ca^{2+} sensor ROD1 (RESISTANCE OF RICE TO DISEASES1) was originally identified as a suppressor of plant immunity, which acts by scavenging reactive oxygen species (ROS) (*24*). Upon pathogen infection, ROD1 is targeted by E3 ubiquitin ligases RIP1 and APIP6 for degradation, which relieves its brake on immunity (*24*). The downstream pathways responsible for the enhanced immunity of *rod1* remain unknown. In this work, we conducted extensive genetic analysis of *rod1* suppressors and established that *OsEDS1* (*enhanced disease susceptibility 1*), *OsPAD4* (*phytoalexin deficient 4*), *OsADR1* (*activated disease resistance 1*), and *OsTIR* (*TIR-only protein*) function downstream of ROD1. The NADase activity of TIR-only protein OsTIR is inhibited by ROD1. In the absence of ROD1, OsTIR produces pRib-AMP and pRib-ADP which promote formation of an OsEDS1-OsPAD4-OsADR1 (EPA) immune complex. Our study thus reveals an immunity brake and trigger mechanism by which a TIR-only protein is surveilled by ROD1 to modulate EPA activation in rice.

Results

Characterization of rod1 *suppressors*

The *rod1* mutant exhibits an autoimmune phenotype and shows strong resistance to rice blast, sheath blight, and bacterial blight (*24*). We performed a genetic screen to identify *suppressors of rod1* (*srd*) by selecting nonstunted plants from large populations of ethylmethanesulfonate (EMS)– and γ-ray–mutagenized *rod1* seeds (Fig. 1A). From the screen, we obtained 18 stable *srd* lines in which the enhanced disease resistance and growth phenotypes of *rod1* were suppressed (Fig. 1B and table S1). Pathogen infection assays showed that the *srd* mutant lines displayed wild-type disease resistance to rice blast *Magnaporthe oryzae* (*M. oryzae*), bacterial blight *Xanthomonas oryzae* pv. *oryzae* (*Xoo*), and sheath blight *Rhizoctonia solani* (*R. solani*) (Fig. 1, C to E). Also, H_2O_2 accumulation and mRNA expression of the defense marker gene *PR1a* were lower in the mutants than in *rod1* (Fig. 1, F and G). These results suggested that ROD1-mediated immune control is dependent on a set of key downstream regulators whose functions are perturbed in the *srd* mutants.

OsADR1, OsPAD4, and OsEDS1 operate downstream of ROD1

To identify causal genes in the *srd* mutants, we performed map-based cloning. We first knocked out (deleted) *ROD1* in *indica* accession Kasalath by CRISPR-Cas9 mutation [*rod1*-KO^{Kasa}, which harbors a 303–base pair (bp) deletion]. The *rod1*-KO^{Kasa} plants were crossed with individual *srd* mutants to generate F_2 mapping populations in which only the *srd* mutations would segregate (Fig. 1A). *SRD3* was located to the *OsADR1* region (fig. S1A). A comparison of *rod1* and *srd3* DNA sequences revealed a single-nucleotide polymorphism (SNP) that changes OsADR1 Ala^{30} to Thr in *srd3* (fig. S1B). The nature of the *srd3* mutant was verified by genetic complementation and an independent CRISPR-Cas9 knockout of *OsADR1* in *rod1* (*OsADR1*-KO) (fig. S1, C to J). By mapping combined with genome sequencing, we uncovered five additional *Osadr1* mutant alleles (*srd1*, *srd2*, *srd5*, *srd11*, and *srd14*) (table S1). All the *Osadr1* mutants are dominant. We speculated that the OsADR1 variants act as a dominant-negative form to interfere with the natural OsADR1.

[1]CAS Center for Excellence in Molecular Plant Sciences, Chinese Academy of Sciences, Shanghai 200032, China. [2]University of the Chinese Academy of Sciences, Beijing 100049, China. [3]School of Life Science and Technology, ShanghaiTech University, Shanghai 201210, China. [4]Ministry of Education Key Laboratory for Biodiversity Science and Ecological Engineering, National Observations and Research Station for Wetland Ecosystems of the Yangtze Estuary, School of Life Sciences, Fudan University, Shanghai 200433, China. [5]School of Life Sciences, Westlake University, Institute of Biology, Westlake Institute for Advanced Study, Hangzhou 310024, China. [6]Department of Plant-Microbe Interactions, Max-Planck Institute for Plant Breeding Research, Carl-von-Linne Weg 10, 50829 Cologne, Germany. [7]School of Pharmaceutical Sciences, Zhengzhou University, Zhengzhou 450001, China. [8]Henan Key Laboratory of Organic Functional Molecules and Drug Innovation, Henan Normal University, Xinxiang 453007, China. [9]College of Agriculture and Biotechnology, Zhejiang University, Hangzhou 310058, China.
*Corresponding author. Email: ywdeng@cemps.ac.cn (Y.D.); yzhang@cemps.ac.cn (Y.Z.); mjgao@fudan.edu.cn (M.G.); zhhe@cemps.ac.cn (Z.H.)
†These authors contributed equally to this work.
‡Present address: College of Resources and Environment and Haixia Institute of Science and Technology, Fujian Agriculture and Forestry University, Fuzhou 350002, China.
§Present address: State Key Laboratory of Plant Genomics, Institute of Microbiology, Chinese Academy of Sciences, Beijing 100101, China.

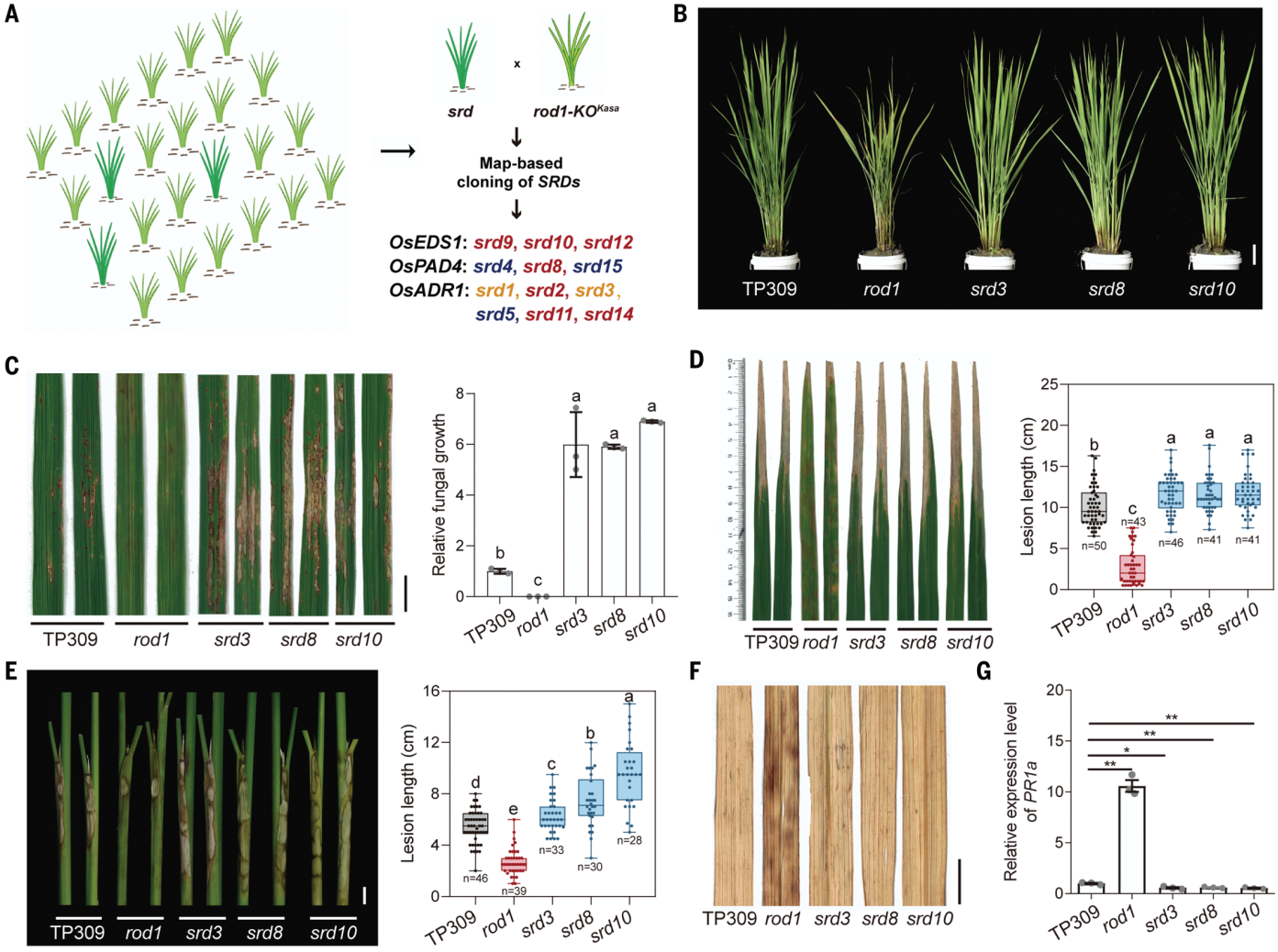

Fig. 1. Genetic reconstitution of the ROD1-EPA immune module in rice. (**A**) An illustration of the genetic screening of *srd* mutants and the characterization of the *SRD* genes. For *OsEDS1*, *OsPAD4*, and *OsADR1* mutation in *srd* plants, red represents a premature stop, orange represents a nonsynonymous substitution, and blue represents a large fragment deletion. (**B**) Photos showing the growth phenotypes of TP309, *rod1*, and representative *srd* mutants. Scale bar is 10 cm. (**C** to **E**) Disease resistance of TP309, *rod1*, and representative *srd* mutants to *M. oryzae* strain TH12 (C), *Xoo* strain PXO99A (D), and *R. solani* isolate RH-9 (E). On the left are photos of inoculation phenotypes. In (C), fungal growth is shown on the right (data are mean ± SD). In (D) and (E), lesion length is shown on the right (*n* indicates the number of biologically independent samples in the graphs; data are displayed as box and whisker plots with individual data points, error bars represent maximum and minimum values, the center line is the median, and box limits are the 25th and 75th percentiles). Significant differences were determined by Duncan's new multiple range test. Lowercase letters indicate statistical significance ($P < 0.05$). Scale bars are 1 cm. (**F**) 3,3′-Diaminobenzidine (DAB) staining in the leaves of TP309, *rod1*, and representative *srd* mutants. Scale bar is 1 cm. (**G**) The expression of the pathogenesis-related gene *PR1a* in TP309, *rod1*, and representative *srd* mutants. Data are mean ± SD ($n = 3$ biologically independent samples). The rice gene *ACTIN1* served as an internal control. Data were analyzed by two-tailed Student's *t* test; $*P < 0.05$, and $**P < 0.01$.

Map-based cloning also identified mutations of *OsEDS1* in *srd9*, *srd10*, and *srd12* (Fig. 1A; fig. S2, A and B; and table S1) and mutations of *OsPAD4* in *srd4*, *srd8*, and *srd15* (Fig. 1A; fig. S3, A and B; and table S1). The mutants were further confirmed by generating CRISPR-Cas9 knockout lines in *rod1* (figs. S2, C to I, and S3, C to I). These comprehensive genetic experiments demonstrate that OsEDS1, OsPAD4, and OsADR1 are essential components of immunity downstream of ROD1 inhibition. We speculated that removal of functional ROD1 releases a brake on immune activation mediated by OsEDS1, OsPAD4, and OsADR1 in rice plants.

OsEDS1, OsPAD4, and OsADR1 promote pattern- and CNL-triggered immunity in rice

The EDS1-PAD4-ADR1 (EPA) node promotes PTI in *Arabidopsis* (*11*, *12*). To test whether OsEDS1, OsPAD4, and OsADR1 function in PTI in rice, we generated *OsADR1*, *OsEDS1*, and *OsPAD4* knockout mutants (*OsADR1*-KO, *OsEDS1*-KO, and *OsPAD4*-KO) in the *japonica* TP309 background (fig. S4A). Compared with wild-type TP309 plants, ROS production was significantly reduced in *OsADR1*-KO, *OsEDS1*-KO, and *OsPAD4*-KO mutants upon chitin PAMP treatment (Fig. 2A and fig. S4B). Moreover, either chitin or the PAMP flg22 could induce expression of *OsADR1* and *OsPAD4* (Fig. 2B), similar to their induction in response to infection with the virulent *M. oryzae* strain TH12 (fig. S4C). Whereas the *OsADR1-KO*, *OsPAD4-KO*, and *OsEDS1-KO* mutants showed compromised resistance to *M. oryzae* TH12, overexpression lines of *OsEDS1*, *OsPAD4*, and *OsADR1* led to enhanced blast resistance compared with wild-type TP309 plants (Fig. 2, C to F). These results

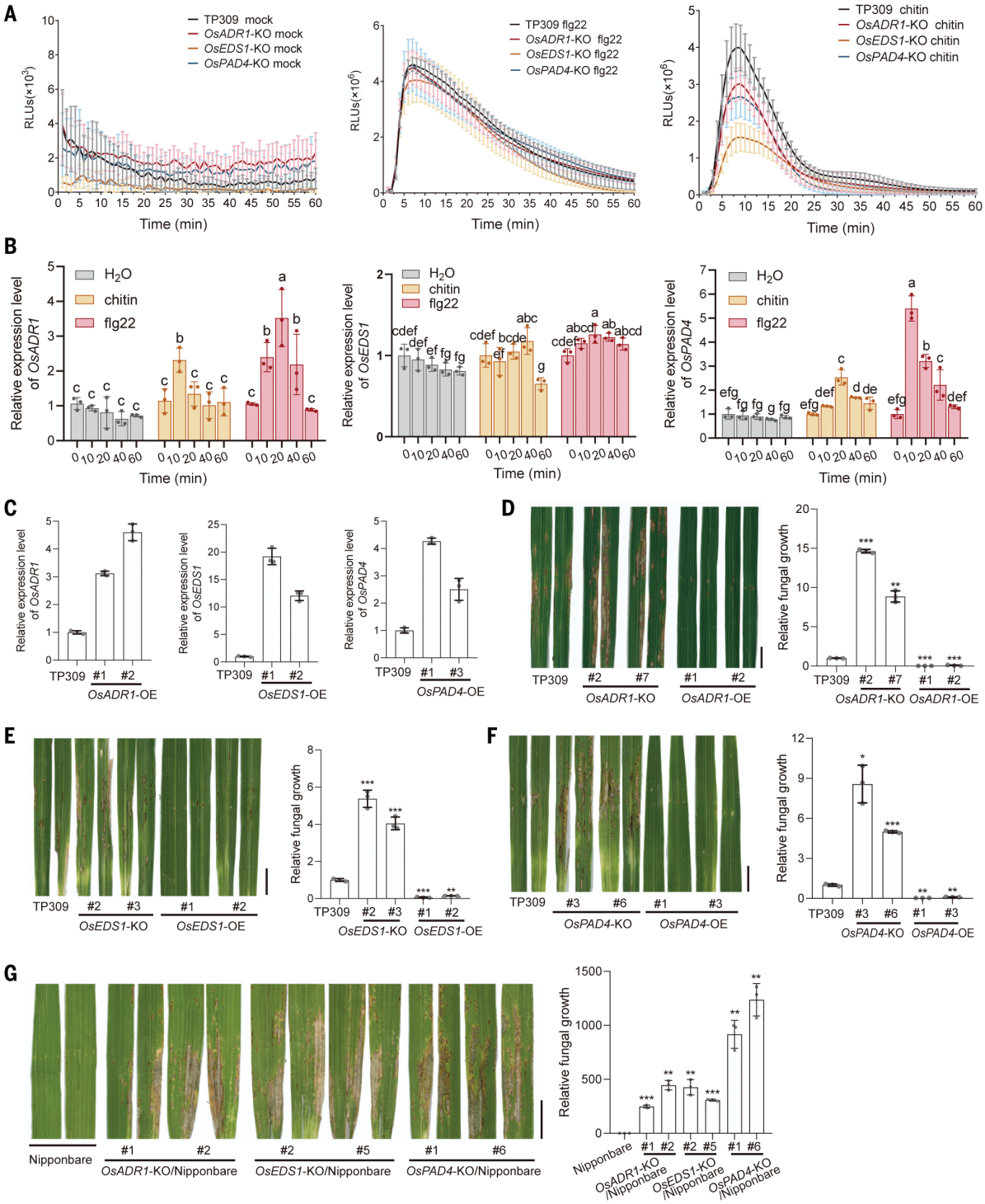

Fig. 2. OsEDS1, OsPAD4, and OsADR1 participate in rice immunity. (**A**) ROS burst detected in wild-type, *OsADR1*-KO, *OsEDS1*-KO, and *OsPAD4*-KO lines in TP309 background treated with ddH_2O, 1 μM chitin, or flg22. Data are mean ± SD ($n = 10$ biologically independent samples). RLUs, relative light units. (**B**) Induction of *OsADR1*, *OsEDS1*, and *OsPAD4* in TP309 upon treatment with 1 μM chitin or flg22, with water used as the control. Data are mean ± SD ($n = 3$ biologically independent samples). The rice gene *ACTIN1* served as an internal control. Significant differences were determined by Duncan's new multiple range test. Lowercase letters denote statistical significance ($P < 0.05$). (**C**) Relative transcript accumulation of *OsADR1*, *OsEDS1*, and *OsPAD4* determined by quantitative reverse transcription polymerase chain reaction (qRT-PCR) in TP309 and OE lines. The rice gene *ACTIN1* served as an internal control. Data are mean ± SD ($n = 3$ biologically independent samples). (**D** to **F**) Disease resistance to *M. oryzae* TH12 was evaluated in wild-type and *OsADR1*-OE/*OsADR1*-KO (D), *OsEDS1*-OE/*OsEDS1*-KO (E), and *OsPAD4*-OE/*OsPAD4*-KO (F) in TP309 background. Shown on the left are photos of inoculation phenotypes. Relative fungal growth is shown on the right. (**G**) Blast resistance of Nipponbare (*Pish*) and representative *OsADR1*-KO, *OsEDS1*-KO, and *OsPAD4*-KO lines in Nipponbare background at 7 days postinoculation with avirulent strain YN2. Shown on the left are photos of inoculation phenotypes. Relative fungal growth is shown on the right. For (D) to (G), data were analyzed using two-tailed Student's *t* test; $^*P < 0.05$, $^{**}P < 0.01$, and $^{***}P < 0.001$. Fungal growth data are mean ± SD ($n = 3$ biologically independent samples). Scale bars are 1 cm.

suggest that OsADR1, OsEDS1, and OsPAD4 contribute to rice PTI regulation.

In *Arabidopsis*, three genetically redundant ADR1 RNL isoforms (ADR1, ADR1-L1, and ADR1-L2) function as helper NLRs in TNL- and some CNL-mediated immune responses (*25*–*27*). To test whether *Os*ADR1 functions similarly in rice, we knocked out *OsADR1* in the *japonica* rice variety Nipponbare, which contains the CNL gene *Pish* that recognizes *M. oryzae* strain YN2 (fig. S4D). *OsADR1*-KO mutant lines displayed reduced *Pish*-mediated blast resistance to strain YN2 compared with wild-type Nipponbare (Fig. 2G and fig. S4E). Moreover, *OsEDS1*-KO and *OsPAD4*-KO mutants also displayed compromised *Pish*-mediated blast resistance (Fig. 2G and fig. S4D). These results suggest that OsADR1 acts as a helper NLR downstream of certain CNLs and that OsEDS1 and OsPAD4 are also required for CNL-mediated ETI in rice.

OsTIR-generated pRib-AMP and pRib-ADP promote EPA complex formation

Upon perception of pRib-AMP and pRib-ADP produced by TNL or TIR-only proteins, the *Arabidopsis* EDS1-PAD4 heterodimer associates with ADR1 to form an activated immune complex (*21*). OsEDS1 constitutively interacted with OsPAD4 (fig. S5, A to D), but neither OsEDS1 nor OsPAD4 interacted with OsADR1 in yeast-two-hybrid (Y2H) and split luciferase complementation (SLC) assays (fig. S5, A and B). We next performed transient coimmunoprecipitation (Co-IP) assays in rice protoplasts and leaves of a *Nicotiana benthamiana eds1a pad4 sag101a sag101b* quadruple (*Nb epss*) mutant (*28*). A weak association between OsADR1 and OsEDS1 or OsPAD4 was detected and was much weaker than that between OsEDS1 and OsPAD4 (fig. S5, C and D), suggesting that assembly of an EPA complex in rice likely involves the TIR-catalyzed small molecules pRib-AMP or pRib-ADP (*21*).

Although the rice genome does not encode TNLs, it contains four *TNP* genes (*OsTNP1-4*, *LOC_Os01g55530*, *LOC_Os08g38970*, *LOC_Os09g30380*, and *LOC_Os11g36760*) and one *TIR-only* gene (*LOC_Os07g37950*, hereafter OsTIR) (Fig. 3A) (*17*). A systematic sequence analysis of the five TIR gene regions in our *srd* mutant populations revealed a Glu^{99}-Asp exchange mutation in *OsTIR* of *srd18* that suppressed the *rod1* autoimmune phenotype (fig. S6, A and C to E). Two independent *OsTIR*-KO/*rod1* mutants also restored *rod1* disease resistance to the same wild-type levels as *srd18* (Fig. 3, B to D, and fig. S6, B to E). The expression of *OsTIR* was induced by pathogen infection (fig. S6F), and the *OsTIR*-KO mutant generated in wild-type TP309 had compromised resistance to *M. oryzae* (fig. S6, G and H). Additionally, ROS production was reduced in the *OsTIR*-KO mutants upon chitin, but not flg22, treatment compared with ROS production in wild-type plants (fig. S6I). We generated knockout lines for two *OsTNP* genes in *rod1* (*OsTNP1*-KO and *OsTNP3*-KO), but this did not affect the autoimmune phenotype of *rod1* (fig. S7). Together, these results establish a genetic link between OsTIR function and ROD1-mediated immune suppression.

Next, using insect cell reconstitution assays, we investigated whether OsTIR induces the OsEDS1-OsPAD4 interaction with OsADR1 to form an EPA complex, as observed with the *Arabidopsis* EPA (*21*). For this, we coexpressed OsTIR with EPA and performed an OsADR1 pull-down assay. A stable EPA complex formed in the presence of OsTIR but not the NADase catalytic mutant $OsTIR^{E133A}$ (Glu^{133}→Ala) (Fig. 3E). Consistent with this finding, OsTIR-triggered cell death in *N. benthamiana* transient expression assays also required its NADase catalytic function (fig. S8A) (*17*). Overexpression of OsTIR in *Nb epss* leaves also promoted EPA complex formation (fig. S8B). To investigate whether OsTIR could generate pRib-AMP and pRib-ADP in insect cells, we performed liquid chromatography coupled with high-resolution mass spectrometry (LC-HRMS) assays. Both molecules were detected in OsTIR-EPA but not in apo-OsEDS1-OsPAD4 (apo-EP) samples lacking OsTIR (Fig. 3F and fig. S9). Furthermore, the addition of synthesized pure pRib-AMP promoted EPA complex formation in *Nb epss* leaves (Fig. 3G). Together, these results indicate that OsTIR catalytically generates pRib-AMP and pRib-ADP, which induce formation of a rice EPA complex.

Structure of the OsEDS1-OsPAD4-OsADR1 immune complex

To understand the structural basis of pRib-AMP/pRib-ADP–induced EPA complex assembly, we coexpressed full-length OsTIR, OsEDS1, OsPAD4, and Flag-tagged OsADR1 (Δ1-156) in insect cells. Affinity purification with anti-Flag resin followed by size-exclusion chromatography yielded a stable EPA complex with a stoichiometric ratio of 1:1:1 (fig. S10A). We determined the structure of the EPA complex at 3.0 Å using a single-particle cryo–electron microscopy (cryo-EM) method (fig. S10, B to E, and table S2). A cryo-EM density map showed unambiguous signals for the full-length OsEDS1-OsPAD4 heterodimer and the C-terminal region of OsADR1, which contains its winged-helix domain (WHD, residues 435 to 550) and C-terminal leucine-rich repeats (LRRs, residues 551 to 859) (Fig. 4, A to C). Notably, a strong map signal was observed between OsEDS1 and OsPAD4 in the EPA complex that fits well with the shape of pRib-ADP (Fig. 4D), consistent with the LC-HRMS data (Fig. 3F) and supporting the enzymatic role of OsTIR in producing pRib-ADP.

pRib-ADP binds at a groove formed by the interface of OsEDS1-OsPAD4, mirroring its binding to the *Arabidopsis* EDS1-PAD4 heterodimer (fig. S11A) (*21*). Also, pRib-ADP–interacting residues of EDS1-PAD4 in the EPA structure are conserved between monocots and dicots (fig. S11B), consistent with pRib-ADP being an immune second messenger in flowering plants (*21*). A structural superimposition of the EPA complex with the apo-AtEDS1-AtPAD4 heterodimer revealed that pRib-ADP induces a similar 20° rotation of the PAD4 C-terminal EP domain (shared by EDS1 and PAD4), removing a steric hindrance and exposing the surface for anchoring OsADR1 (Fig. 4, E and F). In essence, pRib-ADP binds at the same pocket and induces the same conformational change of EDS1-PAD4 in *Arabidopsis* and rice.

Interaction of OsADR1 with OsEDS1-OsPAD4 generates two major interfaces. At the first interface [interface 1 (I1)], a short loop-helix region at the C terminus of OsADR1 interacts with the helix bundle of OsEDS1 and OsPAD4 (Fig. 4G). Residues E850, Y852, W856, and D859 of OsADR1 make H-bond interactions with Q426, R429, K462, and K472 of OsPAD4 (E, Glu; Y, Tyr; W, Trp; D, Asp; Q, Gln; R, Arg; K, Lys). Additionally, van der Waals contacts between OsEDS1 [residues V446 and F449 (V, Val; F, Phe)] and OsADR1 (residues L854 and Y852; L, Leu) appear to enhance their association (Fig. 4G and fig. S12A). The second interface [interface 2 (I2)] involves hydrophobic and polar interactions between the EP domain of OsPAD4 (residues R457, P460, K461, S464, N467, M468, I471, K472, Q475) and the LRR domain of OsADR1 (residues L679, H707, I709, H733, D734, A755, P757, Q779, V781, N782, E803, S805, R806) (P, Pro; S, Ser; N, Asn; M, Met; I, Ile; H, His; A, Ala) (Fig. 4G and fig. S12B). Notably, most residues at the two interfaces are occluded from interaction with ADR1 in the apo-EDS1-PAD4 structure, indicating that there is steric hindrance in the pRib-AMP unbound EDS1-PAD4 dimer that prevents stable ADR1 association. Sequence alignment of residues at these interfaces shows their conservation across different plant species, particularly at the C-terminal short helix of OsADR1 (Fig. 4H and fig. S12C), as observed in the *Arabidopsis* EPA complex (*29*). This suggests that an EPA immune signaling mechanism is conserved across seed plant species and is required for conferring TIR-triggered immunity. Collectively, the data show that OsADR1 contacts the exposed surface on OsEDS1 and OsPAD4 induced by pRib-ADP binding.

ROD1 suppresses OsTIR signaling through the inhibition of TIR NADase activity

To explore a possible molecular link between ROD1 and OsTIR, we tested whether they interact. Co-IP, in vitro pull-down, and SLC assays established that ROD1 interacts directly with OsTIR (Fig. 5, A to C). In *N. benthamiana* transient expression assays, OsTIR-GFP (GFP, green fluorescent protein) mainly localized in the nucleocytoplasm with puncta-like foci formation and colocalized with ROD1 in the cell

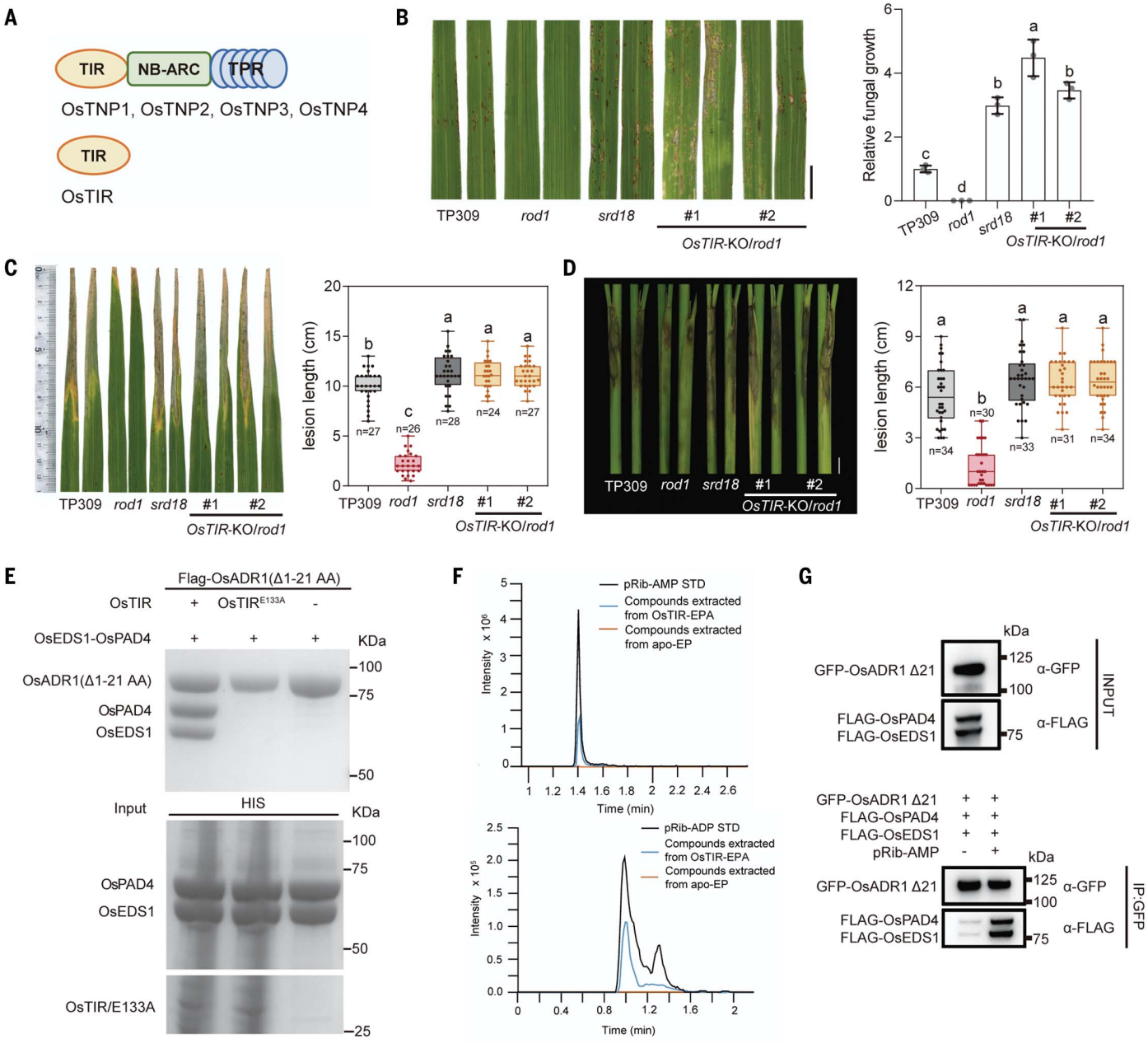

Fig. 3. OsTIR induces OsEDS1-OsPAD4 interaction with OsADR1. (**A**) Schematic presentation of OsTIR and OsTNP proteins in rice. (**B** to **D**) The disease phenotypes (left) of TP309, *rod1*, *srd18*, and *OsTIR*-KO lines in *rod1* were analyzed after inoculation with *M. oryzae* TH12 (B), *Xoo* (C), and *R. solani* (D). Relative fungal growth is shown on the right in (B) (data are mean ± SD; $n = 3$ biologically independent samples), and lesion length is shown on the right in (C) and (D) (*n* indicates the number of biologically independent samples in the graphs; data are displayed as box and whisker plots with individual data points, error bars represent maximum and minimum values, the center line is the median, and box limits are the 25th and 75th percentiles). Lowercase letters denote statistical significance ($P < 0.05$). Scale bars are 1 cm in (B) and (D). (**E**) OsTIR or OsTIR^{E133A} was coexpressed with OsADRI, OsEDSI, and OsPAD4 in insect cells. Proteins purified by flag resins were analyzed by SDS–polyacrylamide gel electrophoresis (SDS-PAGE). (**F**) Chromatograms of supernatant extracts from OsEDS1-OsPAD4-OsADR1 coexpressed with OsTIR (OsTIR-EPA) with retention time 1.40 min, synthesized standard pRib-AMP, and the denatured apo EDS1-PAD4 (top), and chromatograms of supernatant extracts from OsEDS1-OsPAD4-OsADR1 coexpressed with OsTIR (OsTIR-EPA) with retention time 1.00 min, synthesized standard pRib-ADP, and the denatured apo EDS1-PAD4 (bottom). (**G**) Addition of pRib-AMP promotes OsEDS1-OsPAD4 association with OsADR1 in *Nb epss*. Protein input and IP fractions were analyzed by SDS-PAGE. In (E) and (G), experiments were repeated three times with similar results.

periphery (fig. S13), similar to results observed for *Arabidopsis* TIR-domains (*30*). These data point to OsTIR-ROD1 association in the cell periphery. In *N. benthamiana* transient assays, OsTIR-mediated leaf cell death was suppressed by ROD1 (Fig. 5D), consistent with OsTIR-triggered immune responses being inhibited by ROD1. In an in vitro enzymatic assay, OsTIR NADase activity leading to nicotinamide adenine dinucleotide (NAD^+) depletion, and the accumulation of nicotinamide (Nam), ADP ribose (ADPR), and 2′cyclic ADP ribose (2′cADPR) products was compromised in the presence of ROD1 but not the Ca^{2+}-binding mutant ROD1$^{D\text{-}quad}$ (*24*) (Fig. 5E).

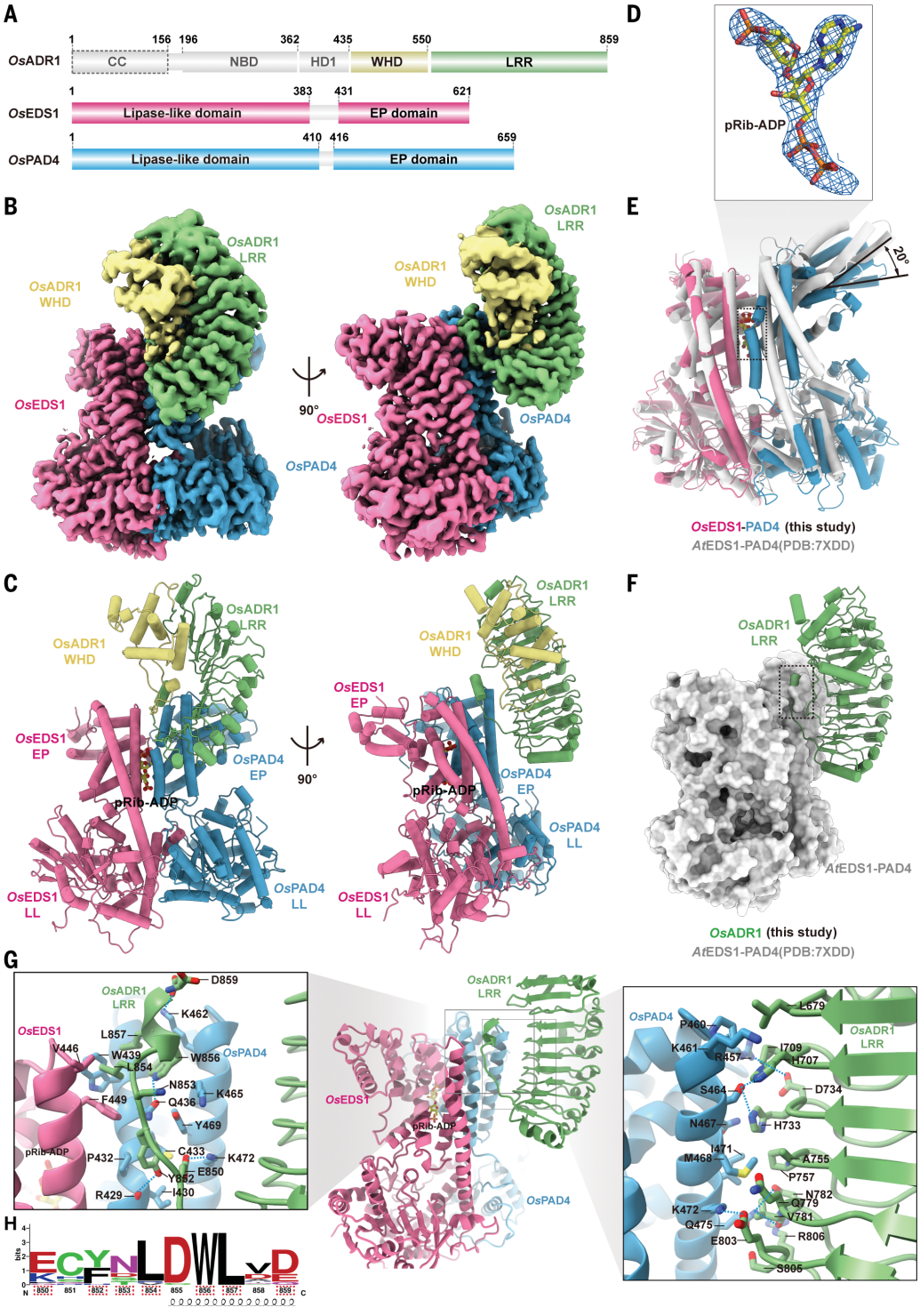

Fig. 4. The cryo-EM structure of the OsEDS1-OsPAD4-OsADR1 immune module. (**A**) Schematic of OsEDS1, OsPAD4, and OsADR1. Gray indicates disordered regions, and the dashed box indicates a truncated region. (**B**) The EPA complex's cryo-EM density map (DeepEMHanced density) in two view orientations. (**C**) The structure model of the EPA complex in two view orientations. (**D**) The cryo-EM density map of pRib-ADP in the structure of the EPA complex. (**E**) Structure superimposition of the AtEDS1-AtPAD4 [Protein Data Bank (PDB) ID 7XDD; gray] (*21*) and the EPA complex. (**F**) Structural modeling of OsADR1 onto the apo AtEDS1-AtPAD4 (PDB ID 7XDD) (*21*) suggests a severe steric clash between the PAD4-EP domain and ADR1. The dashed box highlights steric clash. (**G**) The detailed interaction between OsADR1 and the OsEDS1-OsPAD4 heterodimer. Blue dashed lines indicate hydrogen bonds. (**H**) Sequence logos (*36*) showing the conservation of residues at the C terminus of OsADR1 from different plant species. Residues involved in the interaction with OsADR1 are marked within a red dashed box.

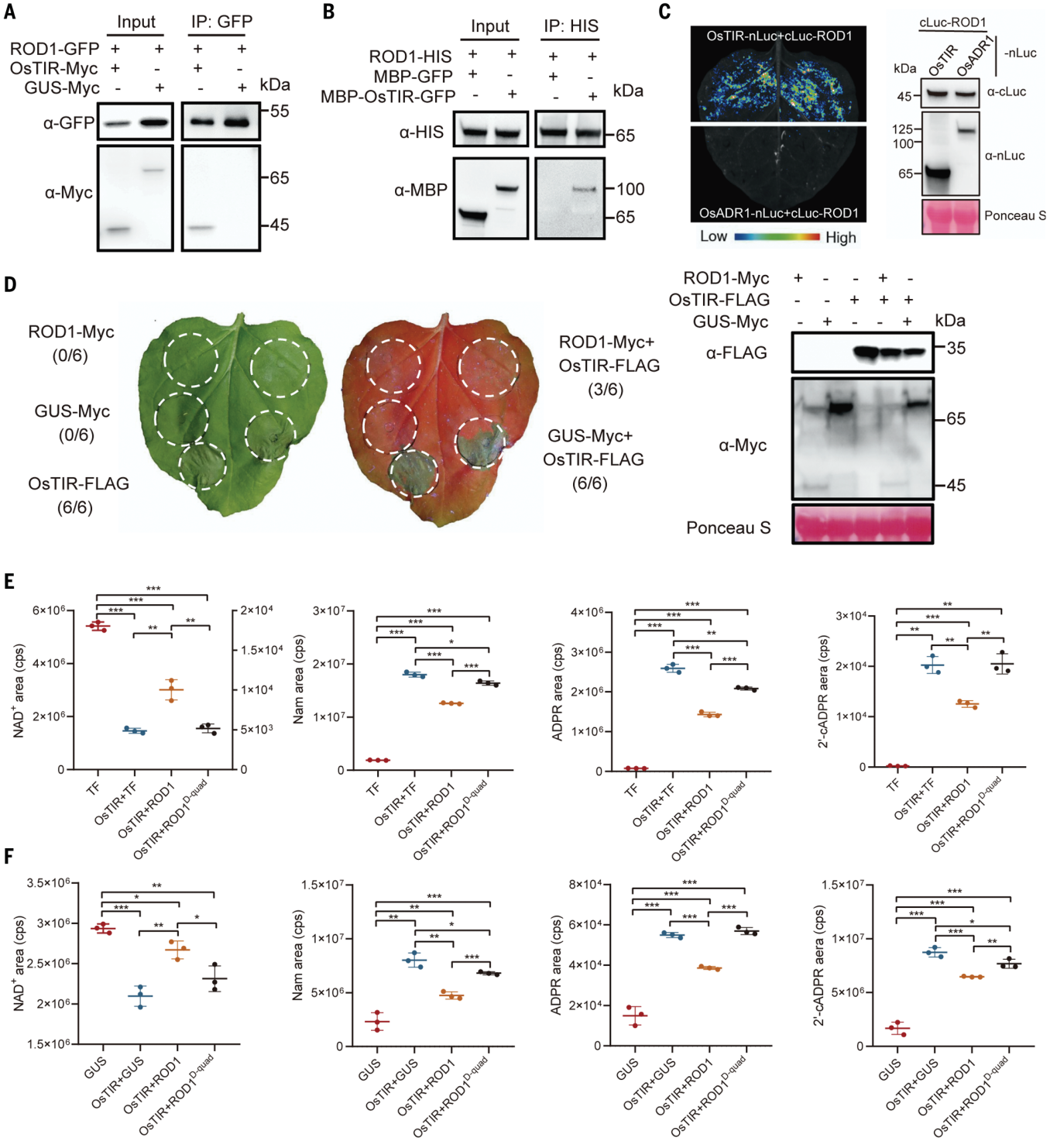

Fig. 5. ROD1 interacts with OsTIR and inhibits its NADase activity. (**A** to **C**) Interaction between ROD1 and OsTIR as detected by Co-IP (A), pull-down (B), and SLC (C) assays. (**D**) Cell death phenotype in *N. benthamiana* leaves. The numbers in parentheses indicate "number of necrotic infiltrated spots/total number of infiltrated spots" (left). The expression of ROD1-Myc, GUS-Myc, and OsTIR-FLAG proteins was confirmed by immunoblot, with Ponceau staining of Rubisco used as a loading control (right). (**E** and **F**) NAD^+ consumption and production of Nam, ADPR, and cyclic ADPR isomer 2′cADPR, detected by LC-HRMS in both in vitro enzymatic assay (E) and in *Nb epss* (F). For NAD^+ consumption in (E), the right three groups refer to the right *y* axis. Data were analyzed using two-tailed Student's *t* test; $^*P < 0.05$, $^{**}P < 0.01$, and $^{***}P < 0.001$. TF, trigger factor; GUS, β-glucuronidase. In (A) to (D), experiments were repeated three times with similar results.

Similarly, coexpression of ROD1 with OsTIR in *Nb epss* leaves suppressed OsTIR-induced NAD^+ depletion and the accumulation of Nam, ADPR, and 2′cADPR (Fig. 5F). These results suggest that ROD1 dampens immune responses in rice in part by associating with OsTIR and inhibiting its NADase activity, thereby limiting the formation of a signaling-active EPA complex.

Discussion

We present evidence for an immune homeostatic mechanism in rice in which ROD1 negatively regulates the OsTIR-EPA defense module to hinder immunity misactivation in uninfected plants. Disabling ROD1 by mutation or pathogen infection (*24*) relieves inhibition of OsTIR, leading to increased OsTIR production of pRib-AMP/pRib-ADP small molecules that directly activate EPA-mediated disease resistance (fig. S14).

The coordinates of rice EDS1-PAD4 dimer amino acids where pRib-AMP/pRib-ADP bind (fig. S11) tally with those determined previously for *Arabidopsis* EDS1-PAD4 (*21*) and in an accompanying structural characterization of the TIR-induced *Arabidopsis* EPA defense module (*29*). The pRib-ADP–bound rice and *Arabidopsis* EDS1-PAD4 dimers display similar PAD4 conformational rotations to expose PAD4 surfaces required for stable interaction with compatible ADR1 C-terminal domains (Fig. 4E) (*29*). Hence, a fundamentally conserved immune-triggering and signal transduction system operates in dicot and monocot plants.

Purification here of TIR-induced stable EPA (1:1:1 heterotrimeric) complexes suitable for cryo-EM analysis required an N-terminally truncated, signaling-inactive rice ADR1 variant (Δ1-156). Other studies suggest that the ultimate functional outcome of TIR- and EP-mediated ADR1 activation in plants is the assembly of oligomeric ADR1 Ca^{2+}-permeable membrane ion channels that would supplement Ca^{2+} channel activities of pathogen-activated CNL oligomers (resistosomes) and thus strengthen the immune response (*31*–*33*). The oligomeric structures formed by EP-activated ADR1-family RNLs, or related NRG1-family RNLs in dicots that cofunction with EDS1-SAG101, are not known.

How a single TIR-only protein is equipped for rice immunity has been unclear. ROD1 is a Ca^{2+} sensor and ROS scavenger (*24*). Because ROD1 directly inhibited OsTIR NADase activity (Fig. 5, E and F), pathogen-induced depletion of ROD1 likely releases OsTIR to respond to ROS and Ca^{2+} stimuli generated by pathogen-triggered PRRs and/or CNLs (*23*). Consistent with this model, the OsTIR-EPA module contributed to immune responses triggered by chitin and flg22 PRR perception and by fungal blast effector–recognizing CNL receptor Pish (Fig. 2, B and G). A released OsTIR NADase enzyme could drive the observed transcriptional up-regulation of *OsTIR* itself and *EPA* genes to further potentiate antipathogen defense (figs. S4C and S6F). Convergence of PRRs and CNL signaling on the OsTIR-EPA module might be especially important in monocot plants that lack potent TNL NADases (*16*).

A further defense-amplifying feature of TIR-only domains is their capacity, via an intrinsically disordered BB-loop, to form subcellular condensates in response to NAD^+ and ATP substrate provision or a pathogen stimulus (*30*). We noted that OsTIR formed cytoplasmic puncta when transiently expressed in *N. benthamiana* leaves (fig. S13A). It is possible these induced OsTIR puncta increase enzymatic production of pRib-ADP/pRib-AMP signals for EPA immune propagation. We measured accumulation of OsTIR-generated NADase nucleotide products in the presence and absence of ROD1 inhibition in vitro and in vivo (Fig. 5, E and F). Although we failed to detect pRib-ADP/pRib-AMP, consistent with previous studies (*21*, *29*), we identified the TIR NADase metabolite 2′cADPR, which can be hydrolyzed to form bioactive EP-binding pRib-AMP, as demonstrated by Yu *et al.* (*29*). Hence, the availability and dynamics of OsTIR NADase cyclic ADPRs also likely affect EPA defense mobilization.

The capacity of rice ROD1 to sense Ca^{2+} and restrict ROS signaling (*24*) and EPA-dependent autoimmunity (Fig. 1) is reminiscent of lesion simulating disease 1 (LSD1) in *Arabidopsis*, which keeps pathogen-induced ROS and EPA defense propagation in check to prevent runaway immune responses (*25*, *34*, *35*). Determining how surveillance proteins such as *Arabidopsis* LSD1 and rice ROD1 integrate pathogen and host signals for balanced TIR-EPA defense will open pathways for improving crop disease resistance and yields.

REFERENCES AND NOTES

1. B. Huot, J. Yao, B. L. Montgomery, S. Y. He, *Mol. Plant* **7**, 1267–1287 (2014).
2. D. Barabaschi, A. Tondelli, G. Valè, L. Cattivelli, *Mol. Plant* **13**, 1352–1354 (2020).
3. Y. Deng *et al.*, *Mol. Plant* **13**, 1402–1419 (2020).
4. Z. He, S. Webster, S. Y. He, *Curr. Biol.* **32**, R634–R639 (2022).
5. D. Couto, C. Zipfel, *Nat. Rev. Immunol.* **16**, 537–552 (2016).
6. J. D. Jones, J. L. Dangl, *Nature* **444**, 323–329 (2006).
7. P. N. Dodds, J. P. Rathjen, *Nat. Rev. Genet.* **11**, 539–548 (2010).
8. B. P. M. Ngou, P. Ding, J. D. G. Jones, *Plant Cell* **34**, 1447–1478 (2022).
9. B. P. M. Ngou, H. K. Ahn, P. Ding, J. D. G. Jones, *Nature* **592**, 110–115 (2021).
10. M. Yuan *et al.*, *Nature* **592**, 105–109 (2021).
11. R. N. Pruitt *et al.*, *Nature* **598**, 495–499 (2021).
12. H. Tian *et al.*, *Nature* **598**, 500–503 (2021).
13. H. Adachi, L. Derevnina, S. Kamoun, *Curr. Opin. Plant Biol.* **50**, 121–131 (2019).
14. L. M. Jubic, S. Saile, O. J. Furzer, F. El Kasmi, J. L. Dangl, *Curr. Opin. Plant Biol.* **50**, 82–94 (2019).
15. J. D. G. Jones, R. E. Vance, J. L. Dangl, *Science* **354**, aaf6395 (2016).
16. D. Lapin, O. Johanndrees, Z. Wu, X. Li, J. E. Parker, *Plant Cell* **34**, 1479–1496 (2022).
17. O. Johanndrees *et al.*, *Plant Physiol.* **191**, 626–642 (2023).
18. S. Ma *et al.*, *Science* **370**, eabe3069 (2020).
19. S. Horsefield *et al.*, *Science* **365**, 793–799 (2019).
20. L. Wan *et al.*, *Science* **365**, 799–803 (2019).
21. S. Huang *et al.*, *Science* **377**, eabq3297 (2022).
22. A. Jia *et al.*, *Science* **377**, eabq8180 (2022).
23. F. Locci, J. E. Parker, *Open Biol.* **14**, 230387 (2024).
24. M. Gao *et al.*, *Cell* **184**, 5391–5404.e17 (2021).
25. V. Bonardi *et al.*, *Proc. Natl. Acad. Sci. U.S.A.* **108**, 16463–16468 (2011).
26. Z. Wu *et al.*, *New Phytol.* **222**, 938–953 (2019).
27. S. C. Saile *et al.*, *PLOS Biol.* **18**, e3000783 (2020).
28. D. Lapin *et al.*, *Plant Cell* **31**, 2430–2455 (2019).
29. H. Yu *et al.*, *Science* **386**, 1413–1420 (2024).
30. W. Song *et al.*, *Nature* **627**, 847–853 (2024).
31. P. Jacob *et al.*, *Science* **373**, 420–425 (2021).
32. J. M. Feehan *et al.*, *Proc. Natl. Acad. Sci. U.S.A.* **120**, e2210406120 (2023).
33. Z. Wang *et al.*, *Proc. Natl. Acad. Sci. U.S.A.* **120**, e2222036120 (2023).
34. C. Rustérucci, D. H. Aviv, B. F. Holt III, J. L. Dangl, J. E. Parker, *Plant Cell* **13**, 2211–2224 (2001).
35. D. Lapin, D. D. Bhandari, J. E. Parker, *Annu. Rev. Phytopathol.* **58**, 253–276 (2020).
36. G. E. Crooks, G. Hon, J. M. Chandonia, S. E. Brenner, *Genome Res.* **14**, 1188–1190 (2004).

ACKNOWLEDGMENTS

We thank J. Chang for providing synthesized pRib-AMP and pRib-ADP; J. Zhou for suggestions on the study; L. Jing and S. Wang for assistance with LC-HRMS assays; L. Kong, Y. Song, G. Li, and J. Duan for cryo-EM data collection at the EM system at the National Facility for Protein Science in Shanghai (NFPS); and X. Men, F. Liu, and S. T. Wang for providing technical support and assistance in cryo-EM data collection at the EM center at Shuimu Biosciences in Hangzhou. **Funding:** This work was supported by the National Natural Science Foundation of China (32088102 and 31930090 to Z.H. and U20A2021 to Y.D.), the National Key Research and Development Program of China (2023YFC2604500 to M.G. and 2022YFE0198100 to Y.D.), Biological Breeding-National Science and Technology Major Projects (2023ZD04070 to Y.D.), the Chinese Academy of Sciences (XDA24010304 to Y.D.), and the Basic Research Zone Program of Shanghai (JCYJ-SHFY-2022-012 to Y.Z.). M.G. is supported by the Shanghai Pujiang Program (22PJ1400700). J.W. and J.E.P. were supported by The Max-Planck Society and Deutsche Forschungsgemeinschaft (DFG) SFB-1403–414786233. Z.H. and J.E.P. acknowledge support from a Sino-German Mobility grant (M-0275). **Author contributions:** Z.H., M.G., Y.Z., and Y.D. conceived the project. Z.H., M.G., Y.Z., Y.D., Y.Wu, and W.X. designed the experiments. Y.Wu, W.X., G.Z., Z.L., and K.L. performed the experiments. J.L., G.Z., X.Z., X.Y., Y.Wa., H.Z., Y.H., Z.Y., and X.W. developed materials and performed genetic analyses. Y.W., W.X., G.Z., Z.L., K.L., S.H., J.W., H.L., and Y.G. analyzed the data. Y.M. and X.C. synthesized the small molecules. J.C. and J.E.P. provided conceptual and experimental advice during the project. Z.H., J.E.P., M.G., Y.Z., Y.D., Y.W., and W.X. wrote the paper. All authors discussed the manuscript. **Competing interests:** The authors declare no competing interests. **Data and materials availability:** All data are available in the main text, supplementary materials, or the listed Protein Data Bank (PDB) files. Atomic coordinates have been deposited into the PDB under accession code 8ZF0 (pRib-ADP–bound OsEDS1-OsPAD4-OsADR1 complex). The EM map for this complex has been deposited in the Electron Microscopy Data Bank under accession code EMD-60049.

SUPPLEMENTARY MATERIALS

science.org/doi/10.1126/science.adr2138
Materials and Methods
Figs. S1 to S14
Tables S1 to S3
References (*37*–*49*)
MDAR Reproducibility Checklist

Submitted 20 June 2024; accepted 18 October 2024
Published online 7 November 2024
10.1126/science.adr2138